Nanotechnology Perceptions
ISSN 1660-6795
www.nano-ntp.com

Composite Nano Lanthanum Aluminate Synthesized by Phytocombustion Method: Energy Storage Devices, Sensing and Biological Applications

Yashaswini[1], R. Venkatesh[1], Y.B. Vinay kumar[2], A.K. Maniyar[3], Kavitha.B.S[4], N. Sivasankara Reddy[5], R. Jagadeesh[6], P. Shankar[7], C.R. Ravikumar[8], A.Jayasheelan[9*]

[1]Department of Physics, BMS Institute of Technology and Management, Bengaluru and affiliated to Visvesvaraya Technological University, Belagavi, India
[2]Department of Information Science and Engineering, BMS Institute of Technology and Management, Bengaluru and affiliated to Visvesvaraya Technological University, Belagavi, India
[3]Department of Physics, BMS College of Engineering, Bengaluru and affiliated to Department of Physics, Mangalore University, Mangalagangotri, India
[4]Department of Physics Government Science College, (Autonomous) Hassan, India
[5]Department of Physics, Presidency University, Bengaluru, India
[6]Department of Chemistry, Maharani Science College for Women, Mysore, India
[7]Department of Physics, Sai Vidya Institute of Technology, Bengaluru, India
[8]Research Centre, Department of Chemistry, East West Institute of Technology, Bengaluru, India
[9]Department of Physics, Maharani Cluster University, Bengaluru, India
Email: jayasheelanwillbe@gmail.com

Materials for energy storage and conversion are essential for the application of nanotechnology. Storage devices must have a long lifespan and are able to store an immense amount of energy in a short span of time. The fabrication of LaAlO3 (Lanthanum aluminate) composite materials through phyto combustion has been examined, using naturally existing Euphorbia-tirucalli-plant latex as fuel. This composite electrode material is being studied as an electrode material for energy storage using cyclic voltammetry and electrochemical impedance spectroscopy (EIS). Additionally, using the disc diffusion method, the produced composite powders' antibacterial efficacy against four bacterial pathogens was investigated. The rhombohedral structure with space group R3m of the pure nano regime is shown by different analytical and spectroscopic techniques. It was found that

the specific capacitance values were 253 Fg-1, 448 Fg-1, and 503 Fg-1.
The creative report reveals a possible option for the creation of super capacitor-like storage devices. Additionally, the use of pure and Bi3+ nanocomposite materials as ascorbic acid and lead sensors is confirmed by their electrochemical behavior. When 30 μg/ml of two gram-positive (Bacillus subtilis, Staphylococcus aureus) and gram-negative (Escherichia coli, Pseudomonas aeruginosa) bacteria were added to the biological activity test, the results revealed very good antibacterial activity. A Two-way ANOVA was used to analyze the data and bi-additive material. The results are shown as *$p < 0.05$ vs. 30 μg/ml of Dy and $p < 0.01$ vs. 20 μg/ml of Dy Sample.

Keywords: Nanocomposite, Phytocombustion synthesis, Supercapacitor, Electrochemical sensing, Antibacterial activity.

1. Introduction

The fundamental source of humanity, energy, is the primary subject of this research. It won't take long for the energy from fossil fuels to run out. It is therefore crucial to find alternate energy sources. To produce energy, however, substantial resources are needed. Therefore, it is necessary to better store and/or save energy for future societies by utilizing modern scientific and technological techniques. This is due to the fact that the demand for energy worldwide is rising daily. Regarding this, the proposed work will highlight recent developments in the production and use of active materials that function in the energy consumption and coordination of renewable energy systems [1]. Nanotechnology is an advanced field that impacts materials at the nanoscale with methodical aid from a variety of industrial and biological approaches [2,3]. The property of a substance changes as its size diminishes, consequently substances with nanoscale dimensions are vital for nanotechnology [4,5].

Owing to their distinctive chemical and physical characteristics, nanomaterials (NMs) are considered suitable materials for an extensive range of applications in fields where energy storage is crucial, including electrochemical (EC), bio-medical sciences, optical, environmental, industrial development, electronics, and supercapacitors [6–7]. It makes sense that the present energy storage trend is a better way to address the global energy dilemma [8].

Applications for nanostructured metal oxides have been widely used in the fields of biological and environmental sciences. Their notable properties such as electrical, biocompatible and EC affirm the effective usage in the manufacturing of supercapacitors and sensors [9-14]. Amidst numerous, lanthanum centered ABO_3 perovskites are exhibiting various advantages like high pitched conduction, extensive voltage, and high stability for charge and discharge pathways. Because of these, perovskite materials are widely used as pseudo-capacitors and are drawn to them due to their notable electrical and magnetic properties. The perovskites primarily regulate the application by cations in the sites of sub lattice.

The most crucial component of supercapacitors, specific capacitance (Csp), increases as a result of these cations' enormous valence electrons forming oxygen vacancies [15]. Supercapacitors are devices that store electrical current and have the benefits of both rechargeable batteries, which provide high energy density, and typical dielectric capacitors, which have a long lifespan [16,17]. Because of their high capacitance, excellent efficiency, quick charge and discharge profiles, affordability, and extended lifespan, lanthanum-based super capacitors are gaining attention [18]. Two electrodes in a supercapacitor are

distinguished electrically by a separator, which is an important component of supercapacitors [19]. Therefore, supercapacitors have been illustrated to be extremely valuable in recent trends related to battery power and electric vehicles, low-emission hybrid vehicles, enhanced power, and load cranes [20-22].

The current work uses trivalent lanthanum (La^{3+}) ions as the A site, transition metal ions Aluminium (Al) as the B site, and rare earth elements Dysprosium and Bismuth ions to build lanthanum aluminate (LA) composites and investigate the EC and biological activity properties. These composites have drawn interest because of their high capacitance, affordability, superior electrode properties, accessibility, and potential for improved performance through a variety of production methods [23-25]. These composite materials can diffuse and transport ions for improved EC applications because of their huge surface area, high crystallinity, more lattice parameter, and high number of oxygen vacancies [26-27].

To verify the nano regime and purity, the produced materials were evaluated using several characterization techniques. Cyclic voltammetry (CV) and galvanostatic charge-discharge in a 6 M KOH electrolyte were used to conduct the EC impedance tests.

2. Experimental methods

2.1. Preparation of $LaAlO_3$ (Lanthanum aluminate) composites utilizing E-tirucalli latex extract

The synthesis was conducted using chemicals $La(NO_3)_3{:}6H_2O$, $Al(NO_3)_3{:}9H_2O$, $Dy(NO_3)_3{:}H_2O$, and $Bi\ (NO_3)_3{:}H_2O$ that were obtained from Sigma Aldrich. E-tirucalli's naturally occurring latex was obtained by marking the plant at Pavagada altitude, which was then employed as fuel for the phytocombustion process [28-29]. Firstly, $LaAlO_3$ sample was prepared by taking a stoichiometric quantity of chemicals and fuel. Prior to gel formation, a gentle mixture of 1:1 nitric acid and distilled water was prepared, then heated on a sand bath. The generated gel and extracted fuel were heated at 350°C in a muffle furnace. Combustion occurs when oxides change into nitrates as gases evolve [30]. The final product was obtained by calcining the acquired product for approximately three hours at 900 ^{0}C. The same methodology had been followed for the fabrication of the other two samples.

2.2. Synthesis of Nanoparticles and impregnated disc dilution

Composite (Dy^{3+} and Bi^{3+}) nanoparticles' (NPs) antibacterial activity was investigated using the paper disc impregnation technique. Four human pathogenic strains of Gram-positive bacteria were employed in the experiment. The bacteria Bacillus subtilis, Staphylococcus aureus, and Gram negative bacteria are known to cause bacteremia, pneumonia, and septicemia, respectively. Enzymes Biosciences Pvt. Ltd., Bengaluru, the biotechnology training institute, provided Escherichia coli (diarrhea, pneumonia) and Pseudomonas aeruginosa (gastrointestinal infections, multiple systemic diseases). Dimethyl sulfoxide (DMSO) was used to dilute the necessary amount of NPs in order to get different concentrations of 5, 10, 20, and 30 μg/ml. Additionally, 6 mm diameter paper discs were created using Whatman No. 1 filter paper and submerged in the previously indicated NPs solution concentrations. By putting these discs on the shaker, the NPs were able to cling to their surface equally.

2.3.Microbiological technique

Following injection into nutrient broth (NB), the cultured bacterial strains are grown on nutrient agar (NA) and maintained at 37 ˚C for approximately 24 hours. The Luria-Bertani agar medium was used to re-inoculate these cultures so as to promote growth. These generated cultures were immediately cultivated in the NB, and their ability was assessed by comparing them to the 0.5 McFarland standard. Using normal protocols, the autoclaved NA/sterilized Mueller-Hinton agar plates were simultaneously prepared for antibacterial activity [31]. Upon solidification, four distinct 25 µl samples of each of the four bacterial strains were spread out on the agar plate. Paper discs were employed in this investigation, and they were soaked with 50 µl of diluted samples and allowed to air dry before being placed on the infected plates. Additionally, paper discs dipped in DMSO served as a negative control, and a positive control for these antimicrobial plates contained ciprofloxacin (10 mcg/disc). After 24 to 36 hours, the diameter of the clear zone of inhibition surrounding the leaf extract-produced discs was measured in millimeters (mm) to determine the antibacterial activity. After three iterations of the analysis, the leaf extract's average region of inhibition diameters (mm) were used to determine the antibacterial activity.

3. Results and discussion

3.1. Characterization

Fig.1 exhibits the PXRD (Powder X-ray diffraction) spectra of the prepared samples concur with the shape, size and strain. The diffraction peaks validate the rhombohedral structure with crystal structure database (JCPDS) card no. 85-1071, utilizing space group R3m and a lattice value of a = 5.35700 Å. The average crystallite sizes of the fabricated samples were estimated by Scherer's equation [32].

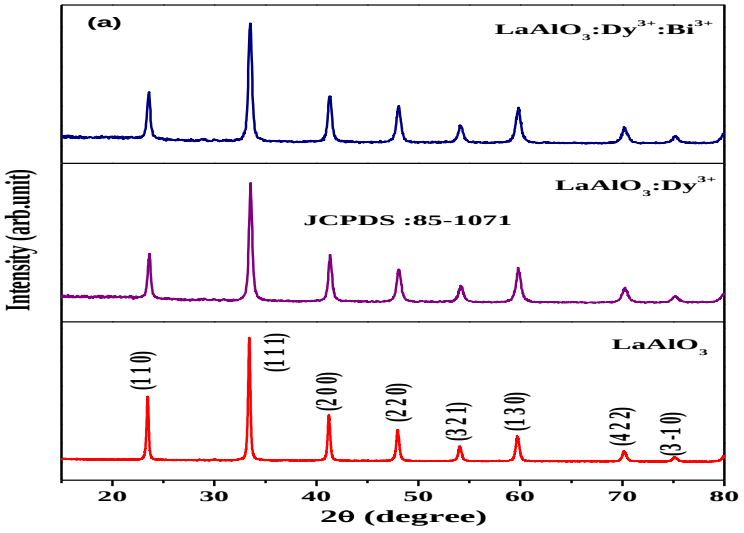

Fig. 1. X-ray diffraction spectra of Lanthanum aluminate and its composite

$$D = \frac{k\lambda}{\beta \cos\theta} \quad (1)$$

The nano regime of materials is confirmed by the estimated crystallite size, which is in the range of 18–28 nm. Additionally, it was noted that the crystal's size reduced from $LaAlO_3$ host lattice to $LaAlO_3$:Dy and $LaAlO_3$:Dy:Bi NMs. This results from an increase in the surface to volume ratio, defects created in the sample by the addition of co-dopants with ionic radii that are much closer to the host lattice (122 pm), and an increase in the number of orbital levels due to orbital shrinkage. The addition of dopants did not affect the structure of the prepared samples. But, the prominent PXRD peak (111) has shifted slightly towards a higher 2θ value.

The FTIR (Fourier Transform Infrared Spectroscopy) is illustrated in Fig. 2 and is used to analyze the chemical bonding and purity of the prepared NMs. The broad absorption peak around 3400 cm^{-1} represents the hydroxyl ions found in all NMs [33], whereas a rather acute peak at about 1602 cm^{-1} was linked to the O-H group's bending. Hence, the O-H bending vibration appears to signify a release mode for lattice species, intended for the tiny quantity of water in the structure. Even after being calcined to a high temperature, the presence of a little amount of H_2O boosts the EC function of battery electrodes. The spectra revealed the vibrational states of the carboxylate ions at 1380 cm^{-1} and the presence of CO_2 molecules at 2431 cm^{-1}. Additionally, the distinct metal oxide peaks measuring 426 cm^{-1}, 677 cm^{-1}, and 825 cm^{-1} were identified [34]. The absence of impurity peaks clearly reveals that the NMs are in its pure form.

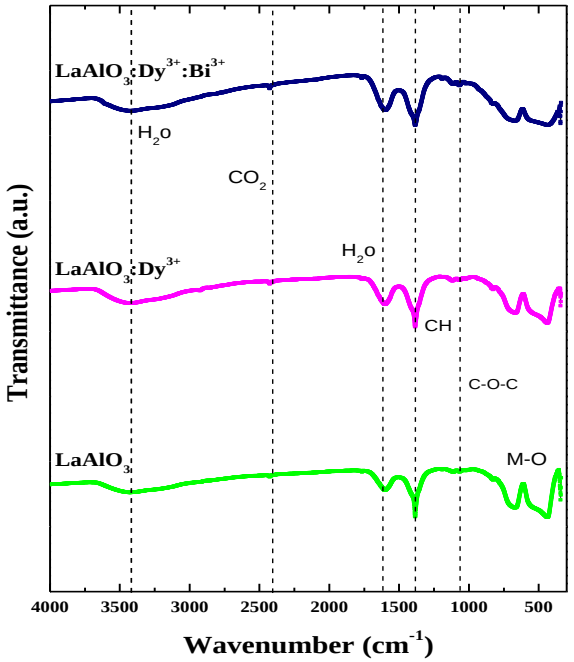

Fig. 2. FTIR spectra of Lanthanum aluminate and its composite

Scanning electron microscopy (SEM) images consents the spongy, uneven fashioned, agglomerated arrangements as shown in Fig.3. The elements and their concentration are

patterned with the help of Energy Dispersive X-ray spectra (EDS) which is attached to the relevant SEM images of Fig.3.

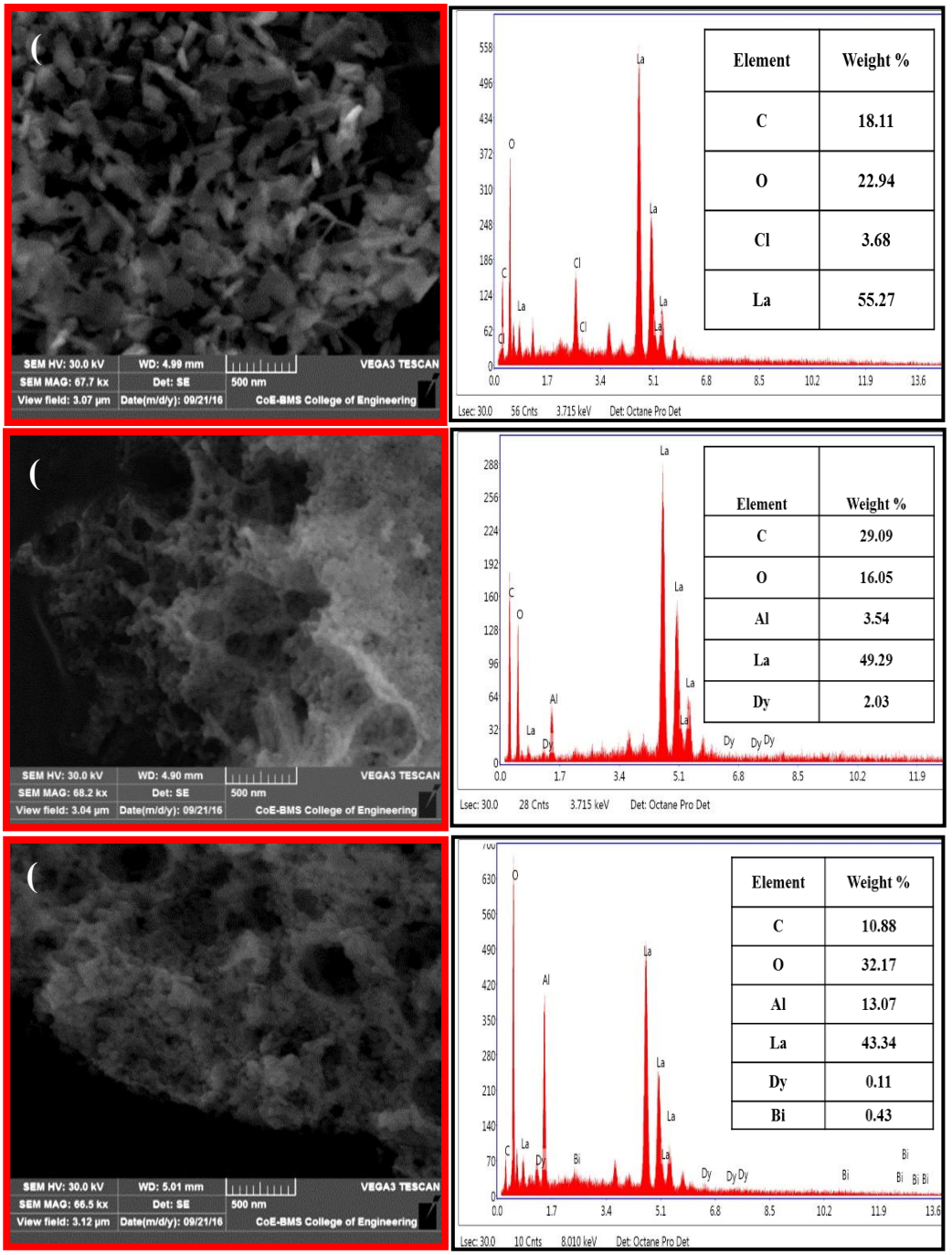

Fig. 3. SEM images attached with EDX spectra of a. $LaAlO_3$ b. $LaAlO_3:Dy^{3+}$ c. $LaAlO_3:Dy^{3+}:Bi^{3+}$ material

Fig. 4, predicts the energy bandgap (E_g)of the NMs estimated using DRS spectroscopy by means of Kubelka-Munk (K-M) model [35].

$$F(R_\infty) = \frac{(1-R_\infty)^2}{2R_\infty} \quad (2)$$

where, F(R) indicates K-M function which is relative to absorption coefficient, R=reflectance,

$$\text{Or} \qquad h\nu = \frac{1240}{\lambda} \quad (3)$$

Band gap energy of the prepared samples were calculated to be 2.77 – 3.10 eV and confirms the increase in trend for the nanocomposite (NC) materials.

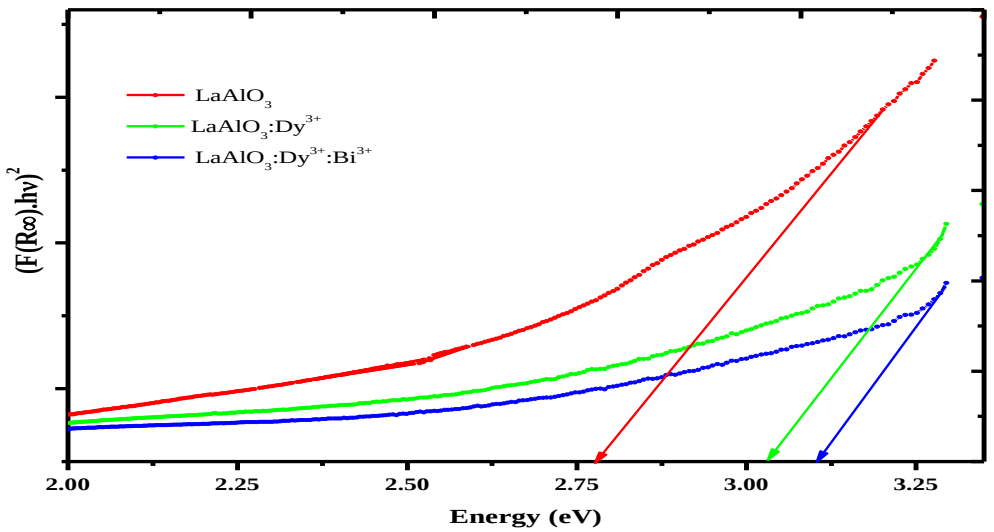

Fig. 4. Optical reflection spectra of Lanthanum aluminate and its composite

3.2. Cyclic voltammetry studies

The studies of cyclic voltammetry (CV) for the synthesized NC materials are shown in Fig. 5, with the scan rate of 10 to 50 mVs^{-1} insteps of 10 mVs^{-1}. In CV two peaks were observed, one for reduction and another for oxidation, which evidences the reduction-oxidation (charge-discharge) behavior of sample electrodes. For different scan rate at -0.3V and 0.4V, the discrete redox experimental peaks represent the better capacitive performance of NC electrode [36-37], which enables the impact of scan rate on the maximum current of NC materials.

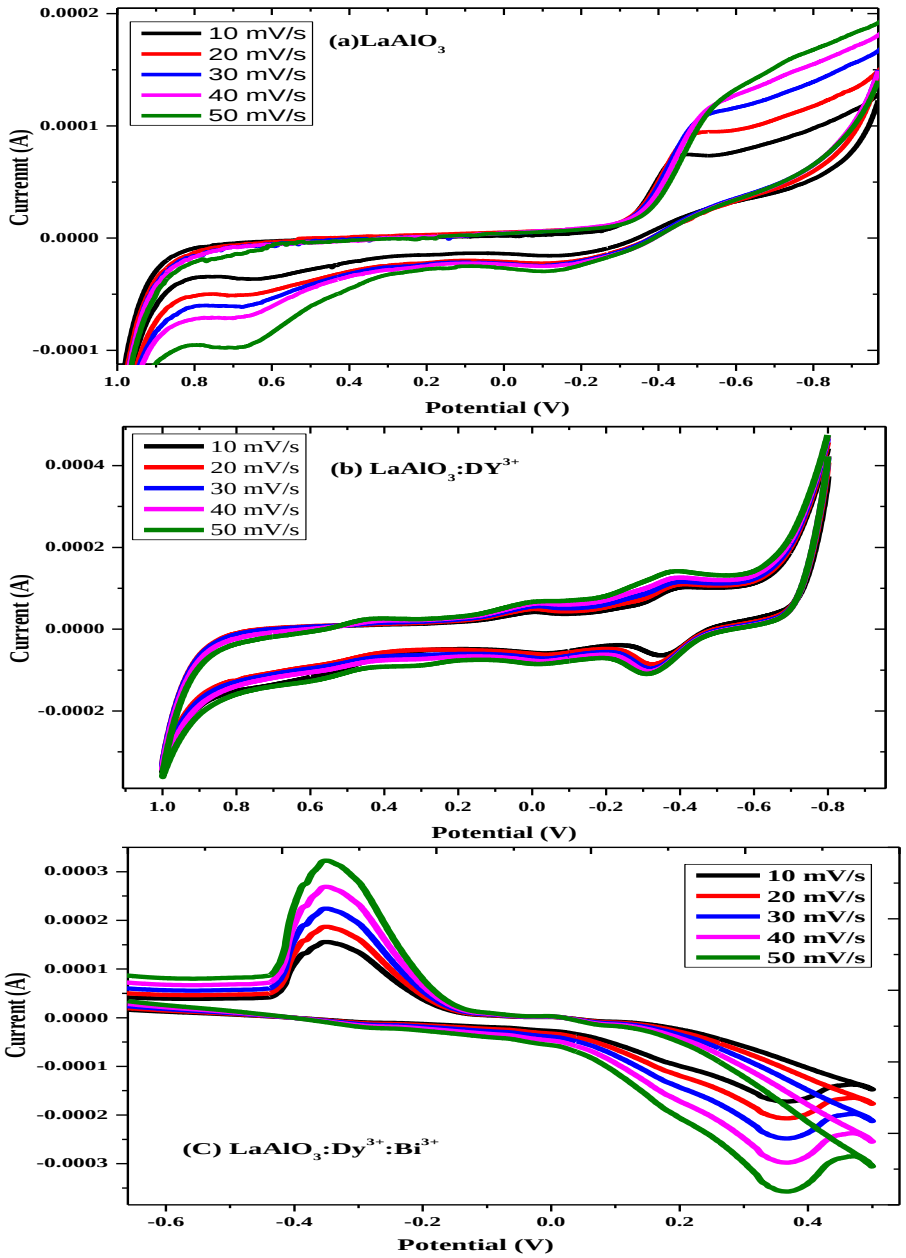

Fig. 5. CV curves of a. $LaAlO_3$, b. $LaAlO_3:Dy^{3+}$, c. $LaAlO_3:Dy^{3+}:Bi^{3+}$ at different scan rates from 10 to 50 mVs-1

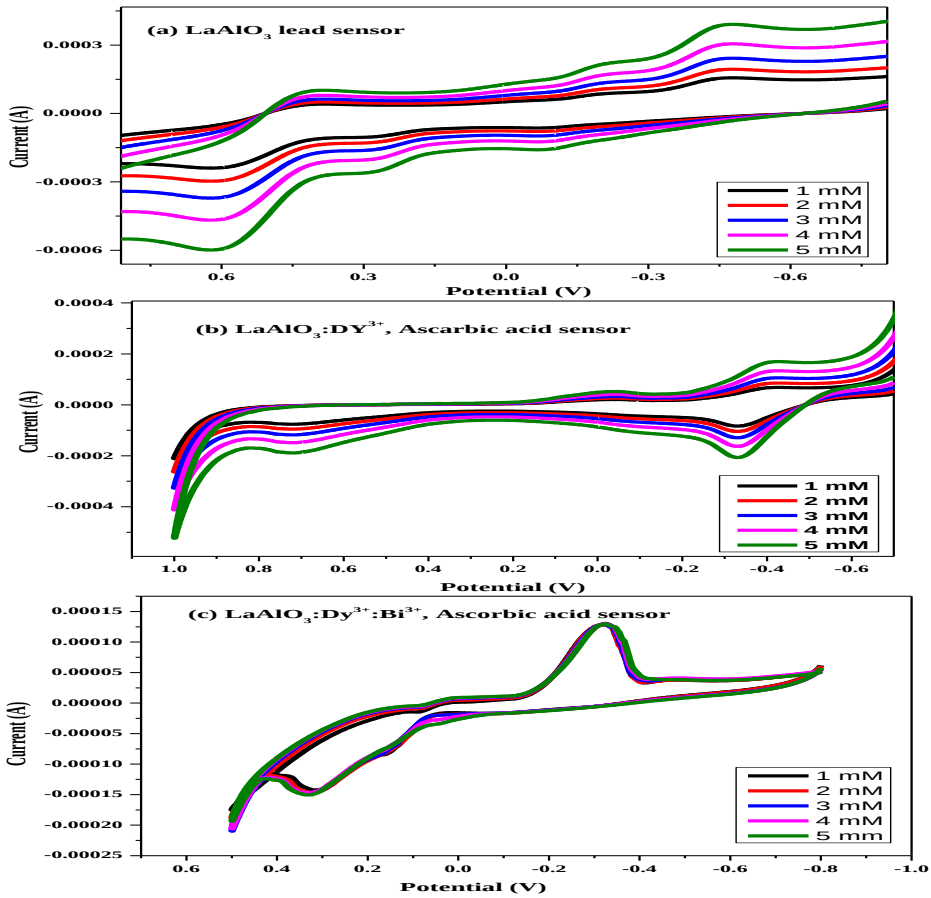

Fig. 6. CV curves of a. $LaAlO_3$, b. $LaAlO_3:Dy^{3+}$, c. $LaAlO_3:Dy^{3+}:Bi^{3+}$ for different concentrations from 1mM to 5mM

During the negative scan, there will be a reduction of AlO_3 from Al^{+3} to Al^{+2}, and the permanence of the +3 state in the presence of the electrolyte is responsible for the for the faradaic behavior of the NC materials during the positive scan of the EC reaction [38]. As the scan rate is increased, the increase in current leads to the capacitance, and redox peaks shift to greater and lesser potential indicates the ohmic resistance and polarization effect of the electrode materials. The observed high current density for Bi^{3+}codoped NM endorses the promising usage as energy storage devices compared other NC materials. The Csp calculated from the equation (4) for pure, Dy^{3+} and Bi^{3+} NC materials are found to be 253 Fg^{-1}, 448 Fg^{-1} and 503 Fg^{-1} respectively for 10 mVs^{-1}scan rate. It was clear that, the decrease in Csp values for the scan rate of 50mVs^{-1} was due to the utilization of inactive material which causes the reduction in capacitance.

Table 1. Value of oxidation potential (E_O), reduction potential (E_R), and difference b/w $E_O - E_R$ of electrodes.

Name of the Electrode	Eo (V)	ER (V)	EO-ER (V)
Pure $LaAlO_3$	0.644	-0.460	1.104

$LaAlO_3$ with Dy^{3+}	0.350	-0.404	0.754
$LaAlO_3$ with Bi^{3+}	0.363	-0.344	0.707

The reversible potential (E_{rev}) can be measured by CV redox peak potentials of the sample electrodes. Though, the reduction (E_C or E_R) and oxidation (E_a or E_O) reaction determines potential distinction ($\Delta E_{a,c}$), the reversible electrode reaction becomes more as value of $E_O - E_R$ is lower. It is evidenced from the table 1 that the reversibility of redox reaction enhances by reducing the $E_O - E_R$ for Bi^{3+}NC material may be due to blocking the pores of the electrodes by Bi^{3+} ion resulting in smooth charge–discharge.

3.3. Lead and Ascorbic Acid EC behavior

Fig.6 illustrates the EC behavior of lead for $LaAlO_3$ and ascorbic acid for composite materials for various concentrations from 1 mM to 5 mM in phosphate buffer solution of pH 7 with a scan rate of 50 mV/s utilizing CV. It is observed that, in all the cases the oxidation and reduction peak current augmented linearly with the increase in concentration. In Bi^{3+} NC material high peak current was observed because of large surface area of the electrode compared Dy^{3+}embedded electrode. This specifies the quick charge transfer on the electrode surface and hence, these pure and NC materials can be used as lead and ascorbic acid sensors.

3.4. Electrochemical impedance spectroscopy

The EC study was assessed by electrochemical impedance spectroscope (EIS) for the frequency range 0.01 Hz to1MHz at 0.3V. Fig.7 Shows the Nyquist plot for the synthesized pure and NC materials. Spectrum displayed straight line equivalent to the imaginary axis representing high capacitance of Bi^{3+} NC compared to pure and Dy^{3+} NC electrodes [39-40]. This may be due to additional free electrons released from the composite element into the conduction band which increases the conductivity [41]. Further, the resistance is almost near to the intercept of real axis which signifies the lower resistance and better conductivity of the electrolyte. It was clear for the figure that, a semicircle for pure and NC materials having decreased trend of diameter clarifies the maximum charge resistance of $LaAlO_3$ electrode (120±5Ω) compared to NC material (49 ± 5Ω).The presence of one semi-circle represents the electrical behavior may be due to grain contribution in the materials [42-43]. It is to be significantly noted that, the charge transfer resistance (49±5Ω) of the electrode surface was decreased and the rate of charge transfer was increased. Similarly, the straight line moves to the smaller frequency region resulting in the higher capacitance of the material [44-46].

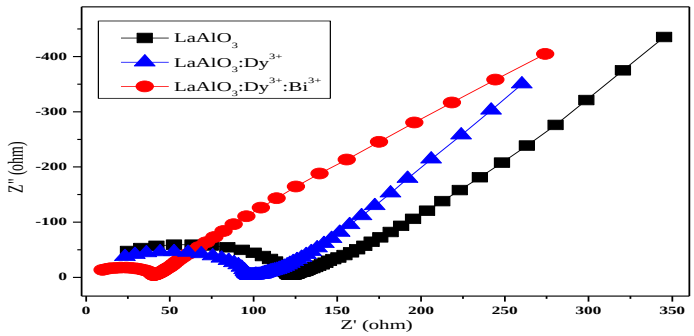

Fig. 7. Nyquist or impedance plots Nano composite materials

As the scan rate is increased, the Csp of the electrode displayed exhibits the decreasing tendency. The Csp of electrodes were estimated by the relation

$$C_{sp} = \frac{\int I\, dV}{V\, m\, \Delta V} \quad (4)$$

Where $\int I\, dV$ is the integrated area of the curve, m is the mass of material on the electrode surface, ΔVis the difference in potential and V is the potential scan rate. The Csp of Bi^{3+} NC electrode reached as high as 503 Fg^{-1} compared to pure and Dy^{3+} NC electrode material. The phase angle near to 90^{o} for frequency up to 0.01 Hz signifies that an optimal capacitor is attained for the NC material of the electrode

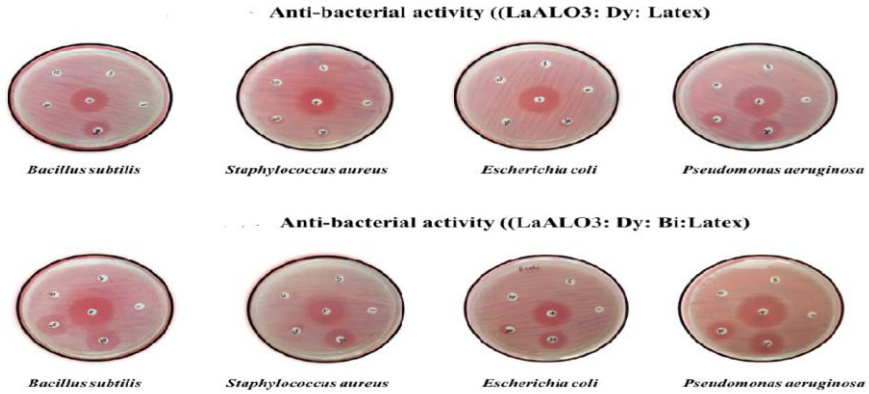

Fig. 8. Antibacterial activity of $LaAlO_3$: Dy and $LaAlO_3$: Dy:Bi nanoparticles using the Disc impregnation method. NP dilution used includes; 5, 10, 20 and 30 µg/ml all samples were diluted using DMSO. Central disc is having Positive Control Chloramphenicol (antibiotic). DMSO is used as Negative Control

3.5. Assay of anti- bacterial activity

The anti-bacterial activity can be concluded based on the zone clearance in each Petri plates. Fig.8 investigated a significant inhibition for Bi^{3+}NC material compared to Dy^{3+} NC material. Though, the zone clearance for Gram Positive bacteria was shown by NC materials for higher concentration, Bi added NC material portrays the significant inhibition for Gram positive and negative bacterial clusters. Although, the work marked the usage of Bi^{3+} NC material (30µg/ml) essentially an effective bactericidal agent against Gram-negative bacteria, since a large number of them are harmful [47].

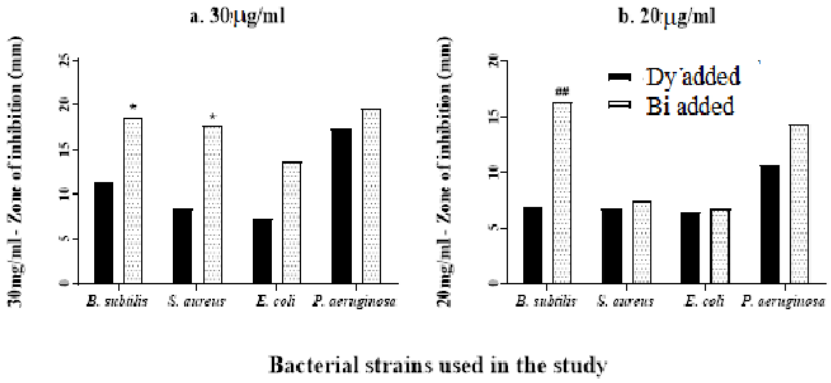

Fig. 9. Inhibition to various pathogenic strains of bacteria at 30 and 20µg/ml concentration

Table 2. Antibacterial activity of different human pathogens again two nanoparticles used in the study, $LaAlO_3$: Dy and $LaAlO_3$: Dy:Bi. Data represented *p<0.05 vs. 30mg/ml of $LaAlO_3$: Dyand $^{\#\#}$p<0.01 vs. 20mg/ml of $LaAlO_3$: Dy

Anti-bacterial activity for $LaAlO_3$: Dy						
Bacterial strains used in the study	Concentration µg/ml 5	10	20	30	Positive	Negative
B. subtilis	0.00	0.00	06.83 ± 0.29	11.33 ± 0.58	21.33 ± 0.58	0.00
S. aureus	0.00	0.00	06.67 ± 0.58	08.33 ± 0.58	25.33 ± 0.58	0.00
E. coli	0.00	0.00	06.50 ± 0.70	07.33 ± 0.57	23.67 ± 1.15	0.00
P. aeruginosa	0.00	0.00	10.66 ± 0.58	17.33 ± 0.58	29.33 ± 0.57	0.00
Anti-bacterial activity for $LaAlO_3$: Dy:Bi						
Bacterial strains used in the study	Concentration µg/ml 5	10	20	30	Positive	Negative
B. subtilis	0.00	0.00	16.33 ± 0.58$^{\#\#}$	18.67 ± 1.15*	27.33 ± 0.58	0.00
S. aureus	0.00	0.00	07.50 ± 0.70	17.66 ± 0.58*	27.33 ± 1.15	0.00
E. coli	0.00	0.00	06.67 ± 0.58	13.67 ± 0.58	22.33 ± 1.53	0.00
P. aeruginosa	0.00	0.00	14.33 ± 0.58	19.66 ± 0.58	26.33 ± 1.52	0.00

4. Conclusion

Effectively prepared the pure and composite samples by solution combustion technique using fuel E-tirucally latex. The characterization of the synthesized materials were performed with XRD, FTIR, and SEM for their size, shape and purity and confirm the nano regime indicating NMs. Band energy gap endorses the insulating nature which can be used as storage devices and dielectric materials. The CV studies measures Csp values which are found to be 253 Fg^{-1}, 448 Fg^{-1} and 503 Fg^{-1} respectively for pure, $Dy^{3+}$and Bi^{3+} NC materials. The high Csp for Bi^{3+} NC can be broadly used in energy storage devices. The EC behavior confirms the usage as an ascorbic acid and lead sensors of pure and Bi^{3+} NC materials respectively. Further, the biological activity was assessed for two-gram positive bacteria (Bacillus subtilis, Staphylococcus aureus) and gram-negative bacteria (Escherichia coli, Pseudomonas aeruginosa) showed significantly good antibacterial activity for 30µg/ml of Bi added composite material and data analyzed by Graph-Pad Prism, Two-way ANOVA and exhibited as *p<0.05 vs. 30µg/ml of Dy and $^{\#\#}$p<0.01 vs. 20µg/ml of Dy Samples.

Credit Authorship Contribution Statement

Yashaswini: Supervision, Investigation, Methodology, Writing, Venkatesh R: Investigation, Methodology, Writing, N.Sivasankara Reddy: Writing, characterization, R.Jagadeesh: Writing, characterization, A.Jayasheelan: Writing – review & editing, C.R. Ravikumar: characterization, Data curation, P.Shankar, A.K.Maniyar, Kavitha.B.S Design

Declaration of Competing Interest

The authors have no known competing financial interests or personal relationships that might have appeared to influence the research work reported in this article

References

1. S. Najib, E. Erdem, Current progress achieved in novel materials for supercapacitor electrodes: mini review, Nanoscale Adv.1(2019)2817–2827.
2. A. Naveen Kumar, D.M. Jnaneshwara, H. Nagabhushana,C.Pratap Kumar, C.R. Ravikumar, M.R. Anil Kumar, T.R. Shashi Shekhar, S.C. Prashantha, Photoluminecence, Photocatalytic, and electrochemical performance of La10Si6O27:Sm3+nanophosphor:It's application in display, photocatalytic and electrochemical sensor. App. Surf. Sci. Adv. 4(2020) 100070.
3. S.Soares e.t al., Nanomedicine: principles, properties, and regulatory issues. Front. Chem. 6, 360(2018)
4. M.AnuM. Saravanakumar, A review on the classification, characterisation, synthesis of nanoparticles and their application. IOP ConfSer Mater Sci Eng. https ://doi.org/10.1088/1757899x/263/3/032019.
5. J. Jeevanandam et al., Review on nanoparticles and nanostructured materials: history, sources, toxicity and regulations.Beilstein J Nanotechno.l9, 1050–1074(2018).https ://doi.org/10.3762/bjnan o.9.98.
6. C.Kang et. Al., Three-dimensional carbon nanotubes for high capacity lithium-ion batteries, J. Power Sources.299, 465–471(2015).https ://doi.org/10.1016/j.jpowsour.2015.08.103.
7. S.Saha et. al., A review on the heterostructure nanomaterials for supercapacitor application. J. Energy Storage. 17:181–202 (2018). https ://doi.org/10.1016/j.est.2018.03.006.
8. D.G. Nocera, Living healthy on a dying planet. Chem.Soc. Rev.38, 13–15(2009). https ://doi.org/10.1039/B8206 60K.
9. LibuManjakkal, DorotaSzwagierczak, RavinderDahiy, Metal oxides based electrochemical pH sensors: Current progress and future perspectives, Prog. Mat. Sci. 109, 100635 (2020)
10. S. Zhuiykov, Solid-state sensors monitoring parameters of water quality for the next generation of wireless sensor networks. Sens.Actuat, B.161, 1–20(2012)
11. L. Manjakkal, C.G. Núñez, W. Dang, R. Dahiya, Flexible self-charging supercapacitor based on graphene-Ag-3D graphene foam electrodes. Nano Energy51, 604–12(2018)
12. W. Dang, L. Manjakkal, W.T. Navaraj, L. Lorenzelli, V. Vinciguerra, R. Dahiya, Stretchable wireless system for sweat pH monitoring. Biosens. Bioelect. 107, 192–202 (2018)
13. M. Viviani, M. T. Buscaglia, V. Buscaglia, M. Leoni, and P. Nanni. Barium perovskites as humidity sensing materials. J. Eur. Cera. Soc. 10-11, 1981-1984 (2001)
14. H. Cao, V. Landge, U. Tata, Y.S. Seo, S. Rao,S.J.Tang, et. al., An implantable, batteryless, and wireless capsule with integrated impedance and pH sensors for gastroesophageal reflux monitoring. IEEE Trans Biomed. Eng.59, 3131–9(2012)
15. M. I. A. Abdel Maksoud, Ramy Amer Fahim, Ahmed Esmail Shalan,, M. Abd Elkodous, S. O. Olojede, Ahmed I. Osman, Charlie Farrell, Ala'a H. Al-Muhtaseb, A. S. Awed, A. H. Ashour, David W. Rooney, Advanced materials and technologies for supercapacitors used in energy

conversion and storage: a review.Env. Chem. Lett. https://doi.org/10.1007/s10311-020-01075-w.
16. A. Halama, B. Szubzda, G. Pasciak, Carbon aerogels as electrode material for electrical double layer supercapacitors—Synthesis and properties, Elect. Chim. Acta. 55, 7501-7505(2010)
17. C. Zhu, Z. Hui, H. Pan, S. Zhu, Q. Zhang, J. Mao, Z. Guo, Y.Li, M. Imtiaz, Z. Chen, Ultrafast Li-ion migration in holey-graphene-based composites constructed by a generalized ex situ method towards high capacity energy storage. J. Mater. Chem. A 7, 4788-4796(2019)
18. J. Sun, et. al., Printable nanomaterials for the fabrication of highperformance supercapacitors. Nanomaterials 8, 528(2018a). https ://doi. org/10.3390/nano8 07052 8.
19. M.A. Pope, et. al., Supercapacitor electrodes produced through evaporative consolidation of graphene oxide-water-ionic liquid gels. J. Elect. Chem. Soc. 160, :A1653–A1660(2013)
20. Z.S. Iro, et. al., A brief review on electrode materials for supercapacitor. Int. J. Elect. Chem. Sci. 11, 10628–10643(2016). https ://doi. org/10.20964 /2016.12.50
21. J.R. Miller, P. Simon, Electrochemical capacitors for energy management. Science 321, 651–652(2008). https ://doi.org/10.1126/science.11587 36.
22. W. Cai, et. al., Transition metal sulfides grown on graphene fibers for wearable asymmetric supercapacitors with high volumetric capacitance and high energy density. Sci. Rep. 6, 26890(2016). https :// doi.org/10.1038/srep2 6890.
23. S. Sahoo, J.J. Shim, Facile Synthesis of Three-Dimensional Ternary ZnCo2O4/Reduced graphene Oxide/NiO composite film on Nickel foam for next generation Supercapacitor electrodes. ACS Sustainable Chem. Eng.5, 241–251(2017)
24. S.B. Patil, M.S. Raghu, B. Kishore, G. Nagaraju, Enhanced electrochemical performance of few-layered MoS2–rGO nanocomposite for lithium storage application, Journal of Mate. Sci.: Mat. in Elect. 30, 316 (2019)
25. K. Yogesh Kumar, Himani Saini, D.Pandiarajan, M.K.Prashanth, L.Parashuram, M.S. Raghu, Controllable synthesis of TiO2 chemically bonded graphene for photocatalytic hydrogen evolution and dye degradation. Catalysis Today, https://doi.org/10.1016/j.cattod.2018.10.042
26. H.S. Nan, et. al., Recent advances in perovskite oxides for anionintercalation supercapacitor: a review. Mat. Sci. Semicond. Proce. 94, 35–50 (2019). https ://doi.org/10.1016/j.mssp.2019.01.033
27. P.P. Ma, et. al., Effect of A-site substitution by Ca or Sr on the structure and electrochemical performance of LaMnO3 perovskite. Elect. Chim. Acta.332. 135489(2020). https ://doi.org/10.1016/j. elect acta.2019.135489.
28. R. Venkatesh, N. Dhananjaya, C. Shivakumara, Effects of monovalent cation doping on the structure and photoluminescence of GdAlO3:Eu3+ phosphor. Int. J. Nanotechnol., Vol. 14, Nos. 9/10/11. 793-800 (2017)
29. S.R. Lakshmi, R. Yadav, R. Venkatesh, M. Raghavendra, T. Ramakrishnappa, N. Dhananjaya, G, Nagaraju, Synthesis of Nano Zna: A Catalyst for N-formylation of Aromatic Amines and Biodiesel Application, Curr. Nanomate. 5, 66-78 (2020)
30. R. Venkatesh, L.S. Reddy Yadav, N. Dhananjaya, A. Jayasheelan, Green combustion synthesis of ZnAl2O4:Eu3+ nanoparticle for photocatalytic activity, Mate. Today: Proce. 49, 583–587(2022)
31. R. Venkatesh, L.S.Reddy Yadav, G. Nagaraju, Ajit Khosla, C. Manjunatha, Antibacterial Study of LaAlO3:Dy3+:Bi3+ Nanoparticles Synthesized by Modified Combustion Technique, ECS Trans. 107 (1), 14985-14992 (2022)
32. T. Ramakrishnappaa, L.S. Reddy Yadava, John Rayan Pereiraa, R. Venkateshb, G. Nagarajuc, Resistivity of zirconium oxide nanoparticles synthesized by solution combustion method using rubber latex fuel. Mat. Today: Proce. 49, 714-719 (2022)
33. R. Venkatesh, L.S. Reddy Yadav, N. Dhananjaya, Rare earth activated bio synthesis of zinc aluminate for photocatalytic activity of dye. Mate. Today: Proce.49, 628-631 (2022)

34. R. Venkatesh, N. Dhananjaya, G. Nagaraju, UdayaBhanu, Rare earth activated and sensitized green synthesis of zinc aluminate for display applications, Int. J. Inno. Engg. Manag. Res.08, 376–381 (2019)
35. L.S. Reddy Yadava, T. Ramakrishnappaa, John Rayan Pereirab, R. Venkateshc, G. Nagaraju, Rubber latex fuel extracted green biogenic Nickel doped ZrO2 nanoparticles and its resistivity. Mate. Today: Proce. 49, 681-685 (2022)
36. T. Desalegn, H.C. Ananda Murthy, C.R. Ravikumar, H.P. Nagaswarupa, Green synthesis of CuO nanostructures using Syzygiumguineense (Willd.) DC plant leaf extract and their applications. J. Nanostruct. 11, 81–94(2021)
37. C.R. Ravikumar, P. Kotteeswaran, V. Bheemaraju, A. Murugan, M.S. Santosh, H. P. Nagaswarupa, S.C. Prashantha, M.R. Anil kumar, M.S. Shivakumar, Influence of zinc additive and pH on the electrochemical activities of β-nickel hydroxide materials and its applications in secondary batteries. J. Energy Storage 9 , 12–24 (2017)
38. R. Kumar, P. Rai, A. Sharma, Facile synthesis of Cu2O microstructures and their morphology dependent electrochemical supercapacitor properties.Rsc. Adv. 6, 3815-3822(2016)
39. N. Arjun, G.T. Thomas. C.K. Yang, The exploration of Lanthanum based perovskites and their complementary electrolytes for the supercapacitor applications.Resu. in Phy. 7, 920-926(2017)
40. [40] R.Venkatesh, S. R. Manohara, G. Nagaraju, N. Dhananjaya, E-tirucalli latex mediated green biogenic synthesized Dy3+ doped and Bi3+ co-doped nano perovskite lanthanum aluminum oxide: structure, morphology, luminescence and dielectric studies. Eur. Phys. J. Plus. 136:948(2021)
41. K. Choudhary, R. Saini, G.K. Upadhyay, V.S. Rana, L.P. Purohit, Wrinkle type nanostructured Y-doped ZnO thin films for oxygen gas sensing at lower operating temperature. Mater. Res. Bull. 141, 111342 (2021).
42. B. Roy, S>Chakrabarty, O. Mondal, M. Pal, A. Dutta, Effect of neodymium doping on structure, electrical and optical properties of nanocrystallineZnO. Mater. Charact. 70, 1–7 (2012)
43. R. Venkatesh, S. Pratibha, N. Dhananjaya, SR. Manohara and G. Nagaraju, Study of optical and dielectric properties of alkalimetal cation (Li+,Na+,K+) codoped Eu3+ activated gadolinium aluminate nanoparticles, Mater.Res.Exp. 6, 095008(2019)
44. B. Shruthi, B.J. Madhu, V. Bheema Raju, S. Vynatheya, B.Veena Devi, G. V. Jayashree, C.R. Ravikumar, Synthesis, spectroscopic analysis and electrochemical performance of modified β-nickel hydroxide electrode with CuO, J. Sci.: Adv. Mater. Devices.2, 93–98(2017)
45. C.R.Ravikumar, M.S. Santosh, H.P. Nagaswarupa, S.C. Prashantha, S. Yallappa, M. R. Anil Kumar, Synthesis and characterization of β-Ni(OH)2 embedded with MgO and ZnO nanoparticles as nanohybrids for energy storage devices, Mater. Res. Express.4, 065503 (2017)
46. B. Avinash, C.R. Ravikumar, M.R. Anil Kumar, H.P. Nagaswarupa, M.S. Santosh, Aarti S. Bhatt, Denis Kuznetsov, Nano CuO: electrochemical sensor for the determination of paracetamol and D-glucose, J. Phys. Chem. Solids.134, 193–200(2019)
47. L. S. Reddy Yadav, B. M. Shilpa, B. P. Suma, R. Venkatesh, G. Nagaraju, Synergistic effect of photocatalytic, antibacterial and electrochemical activities on biosynthesized zirconium oxide nanoparticles, Eur. Phys. J. Plus 136, 764(2021).
48. R.Venkatesh, N. Dhananjaya, M.K. Sateesh, J.P. Shabaaz Begum, S.R. Yashodha, H. Nagabhushana, C. Shivakumara, Effect of Li, Na, K cations on photoluminescence of GdAlO3:Eu3+ nanophosphor and study of Li cation on its antimicrobial activity, J. Alloys and Comp. 732, 725-739(2018)